Chaos-assisted long-range hopping for quantum simulation

Maxime Martinez,[1] Olivier Giraud,[2] Denis Ullmo,[2] Juliette Billy,[3]
David Guéry-Odelin,[3] Bertrand Georgeot,[1] and Gabriel Lemarié[1, 4, 5]

[1] *Laboratoire de Physique Théorique, IRSAMC, Université de Toulouse, CNRS, UPS, France*
[2] *LPTMS, CNRS, Univ. Paris-Sud, Université Paris-Saclay, 91405 Orsay, France*
[3] *Laboratoire Collisions Agrégats Réactivité, IRSAMC, Université de Toulouse, CNRS, UPS, France*
[4] *MajuLab, CNRS-UCA-SU-NUS-NTU International Joint Research Unit, Singapore*
[5] *Centre for Quantum Technologies, National University of Singapore, Singapore*

We present an extension of the chaos-tunneling mechanism to spatially periodic lattice systems. We demonstrate that driving such lattice systems in an intermediate regime of modulation maps them onto tight-binding Hamiltonians with chaos-induced long-range hoppings $t_n \propto 1/n$ between sites at a distance n. We provide numerical demonstration of the robustness of the results and derive an analytical prediction for the hopping term law. Such systems can thus be used to enlarge the scope of quantum simulations in order to experimentally realize long-range models of condensed matter.

Introduction.– In recent years there has been considerable interest in the quantum simulation of more and more complex problems of solid state physics [1–3]. In this context, lattice-based quantum simulation has become a key technique to mimic the periodicity of a crystal structure. In such systems, dynamics is governed by two different types of processes: hopping between sites mediated by tunneling effect and interaction between particles. While there exists several ways to implement long-range interactions [4–7], long-range hoppings have been up to now very challenging to simulate. These long-range hoppings however, have aroused great theoretical interest in condensed matter, as they are associated with important problems such as glassy physics [8], many-body localization [9] or quantum multifractality [10]. In this study we show that such long-range hoppings can be engineered in driven lattices in a moderate regime of modulation.

Temporal driving techniques are widely used in quantum simulation [11], as systems with fast driving can exhibit new topological effects [12–16] and systems with strong driving can mimic disorder [17–22]. In the intermediate regime of modulation we focus on, driven lattices have a classical dynamics which is neither fully chaotic (corresponding to the strong driving case) nor regular (corresponding to the fast driving case), but, as most real-life dynamical systems, show coexistence of chaotic and regular zones in phase space. Our main result is based on the richness of the quantum tunneling effect in such systems: it is known to be *chaos-assisted* [23–35]. This phenomenon is well understood between two regular islands, where it translates into large resonances of the tunneling rate between the two islands when varying a parameter of the system. It has been observed in different experimental contexts, with electromagnetic waves [27, 36–41], and with cold atoms [42–45].

In this paper, we address the generalization of this chaos-assisted tunneling mechanism to the case of a *mixed lattice* composed of regular islands embedded in a chaotic sea, obtained in a moderate regime of temporal driving. We demonstrate that remarkably such a dynamical quantum system can be mapped onto an effective tight-binding Hamiltonian with long-range hoppings $\propto 1/n$, with n the distance between sites. Beyond the intrinsic interest of a new observable quantum chaos effect, our results open new engineering possibilities for lattice-based quantum simulations as they are highly generic, accessible for state-of-the-art experiments and species independent (in the context of cold atoms).

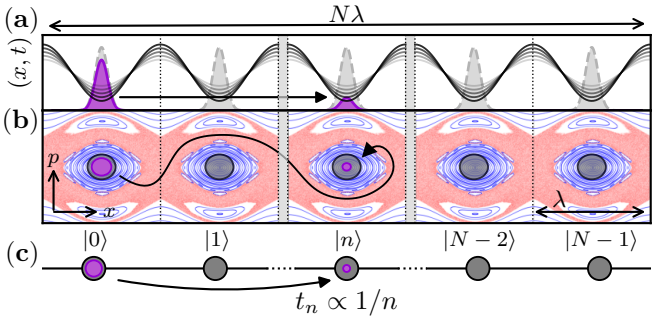

FIG. 1. Equivalent representations of chaos-assisted tunneling in a driven lattice. (a) In situ representation: a wavefunction tunnels through different potential wells. (b) Phase space representation: the wavefunction escapes from an island of stable orbits (blue) by regular tunneling, spreads in the chaotic sea (red) and tunnels in another island. (c) Tight-binding representation: the system is composed of N sites, the coupling between i-th and j-th site is proportional to $1/|i-j|$.

Model.– We consider an experimental situation similar to [45], that is to say a dilute condensate of cold atoms subjected to an optical lattice whose intensity is modulated periodically in time. Using dimensionless variables [46], the dynamics is governed by the Hamiltonian

$$H(x,t) = \frac{p^2}{2} - \gamma(1+\varepsilon\cos t)\cos x. \qquad (1)$$

Here γ is the dimensionless depth of the optical lattice and ε the amplitude of modulation. Importantly, the effective Planck constant $\hbar_{\text{eff}} = -i[x,p] = 2\omega_L/\omega$ can be

tuned experimentally (ω being the modulation angular frequency and ω_L is related to the lattice characteristic energy $E_L = \hbar\omega_L$). This Hamiltonian has a dimensionless time period $T = 2\pi$ and spatial period $\lambda = 2\pi$. Besides the choice of this model, our conclusions are valid for almost any modulation waveform (including phase modulation and kicked potentials).

Semiclassical picture.– The classical dynamics of this time-periodic system is best understood through a stroboscopic phase space, using the values of (x, p) at each period of the modulation $t = jT$, j integer. For $\varepsilon = 0$, the system is integrable. When ε increases, chaos develops close to the separatrix, forming a chaotic sea which surrounds regular islands of oscillating orbits centered around the stable points ($x = 2n\pi$, $p = 0$, n an integer) of the potential wells, see Fig. 1. At $\varepsilon = 0$, with no chaotic sea, tunneling essentially occurs between adjacent wells, and the system can be described for deep optical lattices by an effective tight-binding Hamiltonian with nearest-neighbor hopping. Our main objective is to describe in a similar way the modulated system, a dynamical, spatially periodic lattice of N regular islands indexed by $n \in [\![0, N-1]\!]$, surrounded by a chaotic sea.

Adopting a stroboscopic point of view, the quantum dynamics is described by the evolution operator U_F over one period of modulation. Each eigenstate $|\phi_l\rangle$ of U_F can be associated with a quasi-energy ε_l, so that $U_F|\phi_l\rangle = \exp(-i\varepsilon_l T/\hbar_{\text{eff}})|\phi_l\rangle$. Equivalently the Hamiltonian $H_{\text{strob}} \equiv i(\hbar_{\text{eff}}/T)\log U_F$ gives the exact same stroboscopic dynamics as U_F and is associated with the same eigenstates $|\phi_l\rangle$ with *energies* ε_l.

In the semiclassical regime where $\hbar_{\text{eff}} < \mathcal{A}$, with $\mathcal{A}$ the area of a regular island, the quantum dynamics is strongly influenced by the structures of the classical phase space. Quantum eigenstates can be separated in two types [24, 47]: regular (localized on top of regular orbits) or chaotic (spread over the chaotic sea), see Fig. 2 for a Husimi [48–50] phase-space representation.

The tunnel coupling between regular states is well understood in the case of $N = 2$ regular islands surrounded by a chaotic sea and is called chaos-assisted tunneling [23, 24]. In the absence of a chaotic sea, tunneling involves only a doublet of symmetric and anti-symmetric states localized on the two symmetric islands. In the presence of a chaotic sea, the key property of chaos-assisted tunneling is a 3-level mechanism with one of the regular states interacting resonantly with a chaotic state. This coupling translates in an energy shift of the involved regular state and thus of a strong variation of the original doublet energy splitting (which is nothing but the tunneling frequency). As a signature of the chaotic dynamics, it was shown [23, 25] that these chaos-assisted resonances, observed for the first time in a quantum system only recently [45], occur quite erratically when varying a parameter of the system. Chaos-assisted tunneling involves a purely quantum transport (tunneling to the chaotic sea) and a classically allowed transport (diffusion in the chaotic sea). Thus in mixed lattices, long-range hopping can be expected because the chaotic sea connects all the regular islands across the lattice (see Fig. 1).

Effective Hamiltonian.– The existence of regular islands in the center of each cell (see Fig. 1) motivates the introduction of a set of regular states $\{|n_{\text{reg}}\rangle\}$ forming a lattice with one site per cell, whose exact construction is not crucial for our discussion (see [27] for a detailed discussion). For simplicity, we work in the regime $\hbar_{\text{eff}} \lesssim \mathcal{A}$ such that there is only one regular state by island.

In clear contrast with regular lattices, where only neighboring sites are directly coupled by standard tunneling effect, there exists an *indirect* transfer of probability between distant sites of the modulated lattice due to the mutual coupling with additionnal chaotic states, strongly delocalized along the system. In the original scenario [23], the chaos-assisted tunneling mechanism between regular islands is associated with fast, but weak, probability oscillations between regular islands and the chaotic sea. This picture motivates to capture the physics

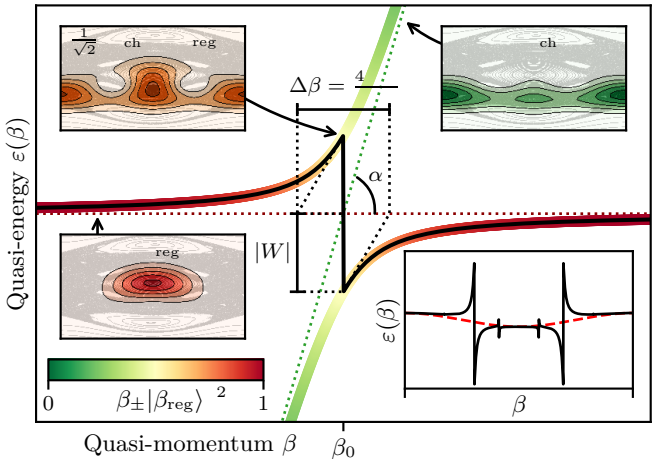

FIG. 2. Sketch of an avoided crossing between regular $|\beta_{\text{reg}}\rangle$ and chaotic $|\beta_{\text{ch}}\rangle$ Bloch waves, showing the different quantities that appear in the two-level model: $|W|$ the strength of the coupling between $|\beta_{\text{reg}}\rangle$ and $|\beta_{\text{ch}}\rangle$, α the slope of the energy of $|\beta_{\text{ch}}\rangle$ and β_0 the point of equal mixing. The width of the crossing $\Delta\beta$ is defined as the intersection of the slope of the energies of mixed states at $\beta = \beta_0$ with the x-axis. Near $\beta = \beta_0$, the eigenstates $|\beta_\pm\rangle$ become a mixture of $|\beta_{\text{reg}}\rangle$ and $|\beta_{\text{ch}}\rangle$ and form two non-crossing branches. As $|\beta_\pm\rangle$ transforms from one original state to the other, the color code gives the intensity of the mixing through the projection of the eigenstate on the regular state $|\beta_{\text{reg}}\rangle$. Solid black line is the effective regular energy (see text). Husimi representations of selected states are given on top of the stroboscopic phase portrait. Inset: Quasi-energy dispersion relation of the Hamiltonian Eq. (1) ($\hbar_{\text{eff}} = 0.4, \gamma = 0.20, \epsilon = 0.15$), black solid line corresponds to the effective regular band and red dashed line to a nearest-neighbor approximation with parameters extracted from the value of the effective regular band at $\beta = 0$ and $\beta = \pi/\lambda$.

of tunneling in our system through an effective Hamiltonian $H_{\rm eff}$, acting only in the regular subspace but generating the same dynamics as $H_{\rm strob}$ in this subspace [51–53]. This effective Hamiltonian can be defined from $(E-H_{\rm eff})^{-1} \equiv P_{\rm reg}(E-H_{\rm strob})^{-1}P_{\rm reg}$, with $P_{\rm reg}$ the projector onto the regular subspace spanned by the $|n_{\rm reg}\rangle$.

In the effective picture, coupling with chaotic states translates in a shift of the energy of each regular Bloch state $|\beta_{\rm reg}\rangle = \frac{1}{\sqrt{N}}\sum_n \exp(i\beta\lambda n)\,|n_{\rm reg}\rangle$ (with β an integer multiple of $2\pi/\lambda N$). The resulting dressed regular band $\varepsilon^{\rm eff}_{\rm reg}(\beta)$ then gives access to the effective tunneling coupling $t^{\rm eff}_n \equiv \langle (m+n)_{\rm reg}|H_{\rm eff}|m_{\rm reg}\rangle$ through the Fourier transform in quasi-momentum

$$t^{\rm eff}_n = \frac{1}{N}\sum_\beta \varepsilon^{\rm eff}_{\rm reg}(\beta)\exp(i\beta\lambda n). \qquad (2)$$

The simplest way to determine the effective spectrum is to start from the full exact spectrum (obtained numerically for instance) and to choose the N most relevant energies. The natural choice is to select energies associated with eigenstates with the largest projection on the regular subspace. In *mixed lattices*, this procedure gives systematic discontinuities in the effective band, coming from accidental degeneracies between a regular $|\beta_{\rm reg}\rangle$ and a chaotic state $|\beta_{\rm ch}\rangle$. Close to such avoided crossings, the branch giving the effective regular energy suddenly changes, resulting in a sharp discontinuity of $\varepsilon^{\rm eff}_{\rm reg}(\beta)$ (see Fig. 2). These sharp discontinuities cause, from property of the Fourier transform in Eq. (2), a long-range decay of the effective coupling term $t^{\rm eff}_n \sim 1/n$ (see Fig. 4).

The two main features of these resonances come from the mixed nature of the system. First, they are sharp because the local slope $\alpha = {\rm d}\varepsilon_{\rm ch}/{\rm d}\beta$ of the crossing state is large since ergodic chaotic states are sensitive to boundary conditions. Second, their heights $2|W| = 2|\langle\beta_{\rm ch}|H|\beta_{\rm reg}\rangle|$ is larger than the regular band width $2|\langle n_{\rm reg}|H|n+1_{\rm reg}\rangle|$ (nearest-neighbor hopping amplitudes for $\varepsilon = 0$, with direct tunneling between islands without chaotic sea).

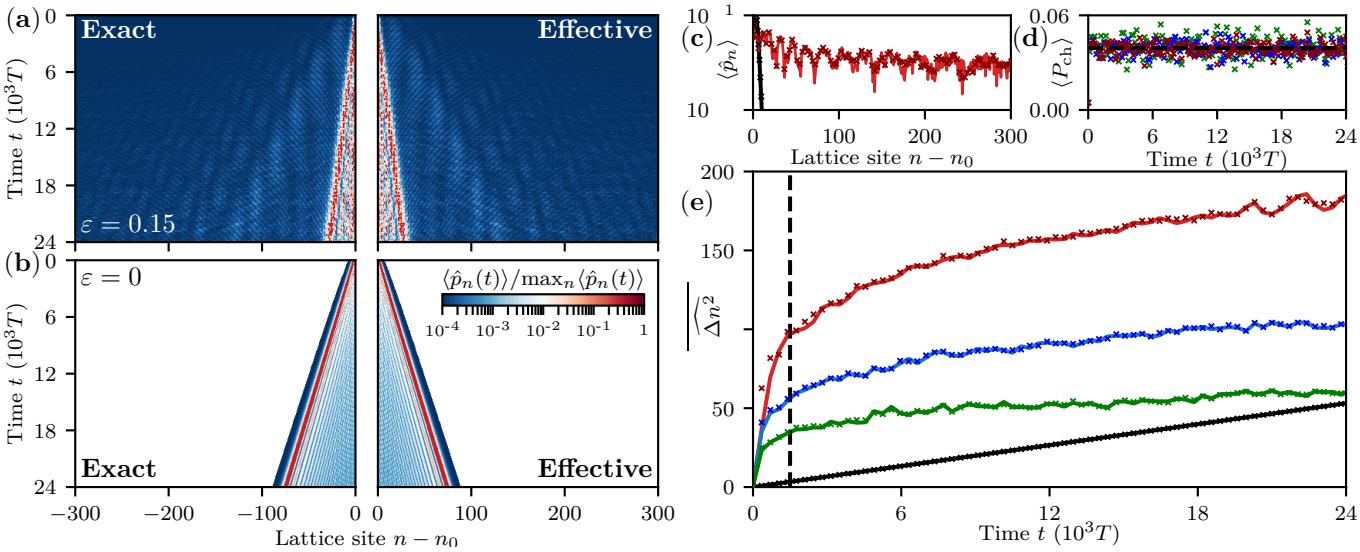

FIG. 3. Dynamics of a wavepacket, initially located on a single regular site n_0. Parameters are $\gamma = 0.2$, $\hbar_{\rm eff} = 0.4$ and $\varepsilon = 0.15$ (modulated lattice) or $\varepsilon = 0$ (unmodulated lattice). (a-b) Probability at each site vs time, normalized for visibility at each time by its maximum value over the lattice. Exact dynamics in the modulated (a) and unmodulated (b) lattices and its corresponding effective dynamics (note that the system is symmetric through $n-n_0 \to n_0-n$). (c) Probability at each site for $t = 1500T$ and $N = 1079$, solid line for exact dynamics and symbols for effective dynamics, red for $\varepsilon = 0.15$ and black for $\varepsilon = 0$. (d) Overlap of the wavefunction with the chaotic sea in the modulated lattice. Same color code as (c), additional blue ($N = 539$) and green ($N = 269$) data for modulated lattices of smaller sizes. (e) Standard deviation of the wavefunction (see text), same color code as (d).

Numerical simulations.– To test the accuracy of this effective tight-binding picture, we compare the exact stroboscopic dynamics with the one given by the effective Hamiltonian, considering a wave packet initially localized on a single regular island of the modulated lattice. (see the Supplemental Material [54] for computational details). As concerns the exact dynamics, the initial condition was chosen to be a localised (Wannier) state of the undriven lattice ($\varepsilon = 0$), in the cell $n_0 = (N-1)/2$, N being odd. We also used the localized states $|n_{\rm reg}\rangle$ to estimate the projection of the wavefunction on the chaotic layer through $P_{\rm ch} \equiv 1 - P_{\rm reg}$. The effective dynamics was studied by propagation of a state initially localized in the cell n_0 of a discrete lattice ruled by the effective Hamiltonian. The effective Hamiltonian was extracted from diagonalization of the Floquet operator on a single cell, for different values of β. In both types of simulations, we defined two observables: a local one $\hat{p}_n$ which enables to

probe the probability at each site, defined as $\hat{p}_n \equiv |n\rangle\langle n|$ in the effective system and $\hat{p}_n \equiv \int_{n\lambda}^{(n+1)\lambda} |x\rangle\langle x|\,\mathrm{d}x$ in the exact system, (this choice was motivated to get $\sum_n \hat{n} = 1$ in both systems) and a global one $\widehat{\Delta n^2} = \sum_n (n-n_0)^2 \hat{p}_n$ to estimate the spreading of the wave function.

We have simulated different system sizes up to $N = 1079$ with periodic boundary conditions and found a very good agreement between the two approaches (see Fig. 3). In the modulated case, we observe a fast and long-range spreading of the wavefunction (Fig. 3a), that is responsible for the tremendous growth of the standard deviation (Fig. 3e). As an additionnal signature of the long-range hopping, the standard deviation appears to saturate with a clear finite size effect, that we attribute to the fact that the boundaries are reached very fast. We have also simulated the exact dynamics of the corresponding undriven lattice with no chaos that highlights the clear contrast between the two systems. Indeed, the unmodulated case gives a slow and short-range ballistic spreading of the wavefunction with no finite-size effect (Fig. 3b and e).

Analytical derivation of the hopping law.– In addition to the expected long-range decay $\propto 1/n$ of the effective coupling term, numerical simulations show apparent erratic fluctuations around this algebraic law (Fig. 4). We discuss here a simple model to explain their origin. For each of the N_{res} resonances in the effective band, we apply a two-level model that involves only three parameters: the slope $\alpha = \mathrm{d}\varepsilon_{\mathrm{ch}}/\mathrm{d}\beta$ of the energy of a chaotic state with β, the coupling intensity W between the chaotic and the regular states and the position β_0 of the crossing in the spectrum (see Fig. 2). Using the linearity of Eq. (2) and assuming sharp resonances ($\Delta\beta \ll 2\pi/\lambda$), the asymptotic behavior of t_n^{eff} is (see Supplemental Material [54])

$$t_n^{\mathrm{eff}} \approx \frac{i}{\pi n} \sum_{\text{resonances}} \mathrm{sgn}(\alpha)|W|\mathrm{e}^{in\beta_0\lambda}. \qquad (3)$$

This simple model is in very good agreement with numerical data (see Fig. 4) and shows that the relevant time scale of the tunneling dynamics is $\hbar_{\mathrm{eff}}/|W|$. The phase term $\mathrm{e}^{in\beta_0\lambda}$, which depends on the position of the resonances in the effective band, gives the observed fluctuations of hopping amplitudes around the algebraic law.

Since the W's of the N_{res} resonances are associated with tunnel coupling to chaotic states, Random Matrix Theory suggests that they can be described as independent Gaussian variables with a fixed variance w^2. In the same spirit, as soon as n is large enough the phases $n\beta_0\lambda$ mod $[2\pi]$ can be considered random. Using the known results about sums of complex numbers with Gaussian amplitudes and random phases [55], Eq. (3) leads to a simple statistical model for the couplings, with $|t_n^{\mathrm{eff}}| \equiv \mathcal{W}/n$ with $\mathcal{W}$ a Gaussian random variable of variance $N_{\mathrm{res}}w^2$. We stress that this implies the distribution of $n|t_n^{\mathrm{eff}}|$ is universal. Fig. 4b shows the validity of this approach.

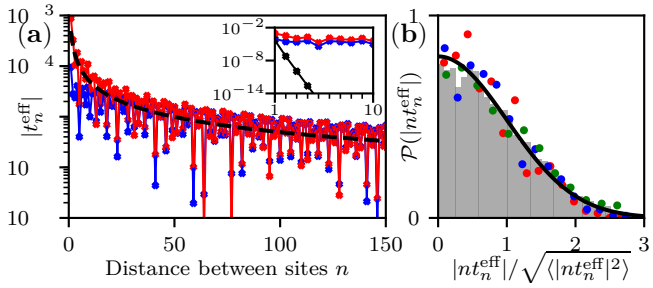

FIG. 4. (a) Effective hopping intensity $|t_n^{\mathrm{eff}}|$ vs distance between sites n for $\gamma = 0.2$, $\varepsilon = 0.15$ and $\hbar_{\mathrm{eff}} = 0.4$. Blue solid line corresponds to the data extracted from numerical Fourier series of the effective band structure. Red solid line corresponds to Eq. (3) with parameters extracted from the band structure. Black solid line is the typical value of Eq. (3). Inset: same data rescaled to show the small-distance behavior, additional black solid line is the unmodulated case $\varepsilon = 0$. (b) Distribution of fluctuations around the $1/n$ law for 5 parameter sets: histogram corresponds to cumulative values for $1500 < n < 10000$, dots are partial datasets of 500 consecutive values of n, black curve is analytical prediction (see text).

Discussion.– The theoretical results presented above rely on the effective Hamiltonian picture. It is thus important to assess its validity in our context. The exact tunneling dynamics between two sites can be written $\langle(n+m)_{\mathrm{reg}}|U_F|m_{\mathrm{reg}}\rangle = \frac{1}{N}\sum_\beta \mathrm{e}^{i\beta\lambda n}\langle\beta_{\mathrm{reg}}|U_F|\beta_{\mathrm{reg}}\rangle$. In the effective approach $\langle\beta_{\mathrm{reg}}|U_F|\beta_{\mathrm{reg}}\rangle$ writes $\exp\!\big(-i\varepsilon_{\mathrm{reg}}^{\mathrm{eff}}(\beta)t/\hbar_{\mathrm{eff}}\big)$, thus it does not take into account the Rabi oscillations of each regular Bloch wave $|\beta_{\mathrm{reg}}\rangle$ with the chaotic sea $|\beta_{\mathrm{ch}}\rangle$, whose amplitude is given in a two-level approximation by $W/\sqrt{W^2+\Delta^2}$ and whose period is $\pi\hbar_{\mathrm{eff}}/\sqrt{W^2+\Delta^2}$ (Δ being the energy difference with the chaotic state involved). The effective picture is thus legitimated by both (1) the sharpness of the resonances that guarantees that the total part of the system that is delocalized in the chaotic sea is small at any time (the amplitude of oscillations being large only close to the resonances), and (2) on the observation that the slowest Rabi oscillation is from Eq. (3) always faster than the induced tunneling process ($\hbar_{\mathrm{eff}}/|t_n^{\mathrm{eff}}| \geq \pi\hbar_{\mathrm{eff}}/W$). These arguments are corroborated by Fig. 3d: the projection of the system on the chaotic sea displays fast and weak oscillations around a very low value.

The arguments we present emphasize that the long-range property is a direct consequence of the existence of sharp and strong tunneling resonances in the band structure, properties which are fairly generic when the classical dynamics of the driven lattice is mixed.

Conclusion.– In this letter we generalized the original chaos-assisted tunneling mechanism between two wells to spatially periodic lattice systems. We demonstrated that in an intermediate regime of temporal driving, the system dynamics could be mapped to a tight-binding Hamilto-

nian with long-range hopping. Strikingly, this new manifestation of chaos at a quantum scale is fairly generic and could be observed in many different experimental situations. In the context of quantum simulation, this result opens the possibility to observe the dynamics of long-range models, and thus to investigate many important phenomena of condensed matter such as glassy physics, many-body localization or quantum multifractality.

This work was supported by Programme Investissements d'Avenir under the program ANR-11-IDEX-0002-02, reference ANR-10-LABX-0037-NEXT, and research funding Grant No. ANR-17-CE30-0024. We thank Calcul en Midi-Pyrénées (CALMIP) for computational ressources and assistance. We thank O. Gauthé and B. Peaudecerf for useful discussions.

[1] I. Bloch, J. Dalibard, and S. Nascimbène, Nature Physics **8**, 267 (2012).
[2] R. Blatt and C. F. Roos, Nature Physics **8**, 277 (2012).
[3] A. Aspuru-Guzik and P. Walther, Nature Physics **8**, 285 (2012).
[4] J. W. Britton, B. C. Sawyer, A. C. Keith, C.-C. J. Wang, J. K. Freericks, H. Uys, M. J. Biercuk, and J. J. Bollinger, Nature **484**, 489 (2012).
[5] R. Landig, L. Hruby, N. Dogra, M. Landini, R. Mottl, T. Donner, and T. Esslinger, Nature **532**, 476 (2016).
[6] C.-L. Hung, A. González-Tudela, J. I. Cirac, and H. J. Kimble, Proceedings of the National Academy of Sciences **113**, E4946 (2016).
[7] H. Busche, P. Huillery, S. W. Ball, T. Ilieva, M. P. A. Jones, and C. S. Adams, Nature Physics **13**, 655 (2017).
[8] D. Sherrington and S. Kirkpatrick, Physical Review Letters **35**, 1792 (1975).
[9] R. M. Nandkishore and S. Sondhi, Physical Review X **7** (2017).
[10] A. D. Mirlin, Y. V. Fyodorov, F.-M. Dittes, J. Quezada, and T. H. Seligman, Physical Review E **54**, 3221 (1996).
[11] A. Eckardt, Reviews of Modern Physics **89**, 011004 (2017).
[12] N. H. Lindner, G. Refael, and V. Galitski, Nature Physics **7**, 490 (2011).
[13] M. C. Rechtsman, J. M. Zeuner, Y. Plotnik, Y. Lumer, D. Podolsky, F. Dreisow, S. Nolte, M. Segev, and A. Szameit, Nature **496**, 196 (2013).
[14] N. Goldman and J. Dalibard, Physical Review X **4**, 031027 (2014).
[15] I.-D. Potirniche, A. Potter, M. Schleier-Smith, A. Vishwanath, and N. Yao, Physical Review Letters **119**, 123601 (2017).
[16] N. Cooper, J. Dalibard, and I. Spielman, Reviews of Modern Physics **91**, 015005 (2019).
[17] G. Casati, B. V. Chirikov, F. M. Izraelev, and J. Ford, in *Stochastic Behavior in Classical and Quantum Hamiltonian Systems*, Vol. 93, edited by G. Casati and J. Ford (Springer-Verlag, Berlin/Heidelberg, 1979) pp. 334–352, series Title: Lecture Notes in Physics.
[18] S. Fishman, D. R. Grempel, and R. E. Prange, Physical Review Letters **49**, 509 (1982).
[19] R. Graham, M. Schlautmann, and D. L. Shepelyansky, Physical Review Letters **67**, 255 (1991).
[20] F. L. Moore, J. C. Robinson, C. F. Bharucha, B. Sundaram, and M. G. Raizen, Physical Review Letters **75**, 4598 (1995).
[21] G. Casati, I. Guarneri, and D. L. Shepelyansky, Physical Review Letters **62**, 345 (1989).
[22] J. Chabé, G. Lemarié, B. Grémaud, D. Delande, P. Szriftgiser, and J. C. Garreau, Physical Review Letters **101**, 255702 (2008).
[23] S. Tomsovic and D. Ullmo, Physical Review E **50**, 145 (1994).
[24] O. Bohigas, S. Tomsovic, and D. Ullmo, Physics Reports **223**, 43 (1993).
[25] F. Leyvraz and D. Ullmo, Journal of Physics A: Mathematical and General **29**, 2529 (1996).
[26] A. Shudo, Y. Ishii, and K. S. Ikeda, EPL (Europhysics Letters) **81**, 50003 (2008).
[27] A. Bäcker, R. Ketzmerick, S. Löck, M. Robnik, G. Vidmar, R. Höhmann, U. Kuhl, and H.-J. Stöckmann, Physical Review Letters **100**, 174103 (2008).
[28] A. Bäcker, R. Ketzmerick, S. Löck, and L. Schilling, Physical Review Letters **100** (2008).
[29] S. Löck, A. Bäcker, R. Ketzmerick, and P. Schlagheck, Physical Review Letters **104** (2010).
[30] O. Brodier, P. Schlagheck, and D. Ullmo, Physical Review Letters **87**, 064101 (2001).
[31] O. Brodier, P. Schlagheck, and D. Ullmo, Annals of Physics **300**, 88 (2002).
[32] N. Mertig, S. Löck, A. Bäcker, R. Ketzmerick, and A. Shudo, EPL (Europhysics Letters) **102**, 10005 (2013).
[33] A. Mouchet, C. Miniatura, R. Kaiser, B. Grémaud, and D. Delande, Phys. Rev. E **64**, 016221 (2001), publisher: American Physical Society.
[34] A. Mouchet and D. Delande, Physical Review E **67** (2003).
[35] S. Keshavamurthy and P. Schlagheck, *Dynamical Tunneling - Theory and experiment* (2011).
[36] C. Dembowski, H.-D. Gräf, A. Heine, R. Hofferbert, H. Rehfeld, and A. Richter, Physical Review Letters **84**, 867 (2000).
[37] R. Hofferbert, H. Alt, C. Dembowski, H.-D. Gräf, H. L. Harney, A. Heine, H. Rehfeld, and A. Richter, Physical Review E **71**, 046201 (2005).
[38] S. Gehler, S. Löck, S. Shinohara, A. Bäcker, R. Ketzmerick, U. Kuhl, and H.-J. Stöckmann, Physical Review Letters **115**, 104101 (2015).
[39] S. Shinohara, T. Harayama, T. Fukushima, M. Hentschel, T. Sasaki, and E. E. Narimanov, Physical Review Letters **104**, 163902 (2010).
[40] M.-W. Kim, S. Rim, C.-H. Yi, and C.-M. Kim, Optics Express **21**, 32508 (2013).
[41] B. Dietz, T. Guhr, B. Gutkin, M. Miski-Oglu, and A. Richter, Physical Review E **90**, 022903 (2014).
[42] W. K. Hensinger, H. Häffner, A. Browaeys, N. R. Heckenberg, K. Helmerson, C. McKenzie, G. J. Milburn, W. D. Phillips, S. L. Rolston, H. Rubinsztein-Dunlop, and B. Upcroft, Nature **412**, 52 (2001).
[43] D. A. Steck, Science **293**, 274 (2001).
[44] D. A. Steck, W. H. Oskay, and M. G. Raizen, Physical Review Letters **88** (2002).
[45] M. Arnal, G. Chatelain, M. Martinez, N. Dupont, O. Giraud, D. Ullmo, B. Georgeot, G. Lemarié, J. Billy, and D. Guéry-Odelin, Science Advances **6**, eabc4886 (2020).

[46] $p = 2\pi P/(M\omega d)$, $x = 2\pi X/d$ where P and X are the momentum and position along the optical lattice, M is the atomic mass, d is the lattice spacing, and the time t is measured in unit of the modulation angular frequency ω.
[47] M. V. Berry, Journal of Physics A: Mathematical and General **10**, 2083 (1977).
[48] K. Husimi, Proceedings of the Physico-Mathematical Society of Japan. 3rd Series **22**, 264 (1940).
[49] M. Terraneo, B. Georgeot, and D. L. Shepelyansky, Phys. Rev. E **71**, 066215 (2005).
[50] S.-J. Chang and K.-J. Shi, Physical Review A **34**, 7 (1986).
[51] H. Feshbach, Annals of Physics **5**, 357 (1958).
[52] H. Feshbach, Annals of Physics **19**, 287 (1962).
[53] P. Löwdin, Journal of Mathematical Physics **3**, 969 (1962).
[54] See Supplemental Material at [URL will be inserted by publisher] for computational details and analytical derivation of the hoping law Eq. (3), which includes Refs. [45, 49].
[55] P. Beckmann, Journal of Research of the National Bureau of Standards, Section D: Radio Propagation **66D**, 231 (1962).

Supplementary material for Chaos-assisted long range hopping for quantum simulation

Maxime Martinez,[1] Olivier Giraud,[2] Denis Ullmo,[2] Juliette Billy,[3]
David Guéry-Odelin,[3] Bertrand Georgeot,[1] and Gabriel Lemarié[1, 4, 5]

[1] *Laboratoire de Physique Théorique, IRSAMC, Université de Toulouse, CNRS, UPS, France*
[2] *LPTMS, CNRS, Univ. Paris-Sud, Université Paris-Saclay, 91405 Orsay, France*
[3] *Laboratoire Collisions Agrégats Réactivité, IRSAMC, Université de Toulouse, CNRS, UPS, France*
[4] *MajuLab, CNRS-UCA-SU-NUS-NTU International Joint Research Unit, Singapore*
[5] *Centre for Quantum Technologies, National University of Singapore, Singapore*

In this Supplementary material, we describe the methods used to numerically simulate the dynamic evolutions of the temporally modulated system and of the effective Hamiltonian, whose construction we explain in more details. The code we used is written in Python 3 and uses the Numpy library. It is available at https://framagit.org/mmartinez/dynamics1d. We then describe in detail the derivation of the hopping law.

Numerical methods

Exact dynamics of the periodically modulated lattice

The system, composed of N_c cells of spatial size $\lambda = 2\pi$ is discretized with N_p points per cell; the total basis size is thus $N_t = N_c N_p$. We have used both a spatial $|x\rangle$ and momentum $|p\rangle$ representation. The corresponding grids are centered around $x = 0$ and $p = 0$ with respective size-step:

$$\delta x = \frac{\lambda}{N_p} \quad \text{and} \quad \delta p = \frac{2\pi}{\lambda}\frac{\hbar_{\text{eff}}}{N_c}. \tag{1}$$

For the whole of the study, we took $N_p = 32$ after checking that this discretatization was fine enough to faithfully represent the dynamics of the system: in particular, the total size in the p direction $N_p\hbar_{\text{eff}}$ should be larger than the extension of the chaotic sea in momentum space.

The time propagation of a given state $|\psi\rangle$ is achieved with a symmetrized split-step method:

$$|\psi(t+\delta t)\rangle = U_P F U_X F^{-1} U_P \,|\psi(t)\rangle\,, \tag{2}$$

with

$$U_X = \sum_x \exp\left(-i\frac{V(x,t)\delta t}{\hbar}\right)|x\rangle\langle x|\,,\ U_P = \sum_p \exp\left(-i\frac{p^2\delta t}{4\hbar}\right)|p\rangle\langle p| \tag{3}$$

$$F = \frac{1}{\sqrt{N}}\sum_{x,p}\exp\left(-i\frac{xp}{\hbar}\right)|p\rangle\langle x| \quad \text{(using FFT)}. \tag{4}$$

The time step $\delta t = 4\pi/1000$ was chosen after consistency tests.

Construction of the effective Hamiltonian

The determination of the Floquet-Bloch band is equivalent to the determination of the quasi-energy spectrum of the following Hamiltonian

$$H_\beta(x,t) = \frac{(p-\hbar_{\text{eff}}\beta)^2}{2} - \gamma(1+\varepsilon\cos t)\cos x, \tag{5}$$

on a single cell $N_c = 1$ (with $N_p = 32$, see above), with the quasi-momentum β taking the discrete values $\beta_m = 2\pi m/(N_c\lambda)$, $m = 0, \ldots, N_c - 1$. Thus, for a system size N_c, we repeat N_c times the following procedure (for each value of β_m):

- First, we build the matrix (in x reprentation) of the Floquet operator from the propagation of N_p δ-function states $|x\rangle$. To do so, we use the previous split-step method over two periods of modulation $T = 4\pi$ (this choice was made to be consistent with [1], but is of no importance here).
- Second, we diagonalize the Floquet operator and look for the eigenstate having the largest overlap with a Gaussian state centered on the regular island. This eigenstate is associated with a complex eigenvalue α_β that gives the effective energy:

$$\varepsilon_{\text{eff}}^{\text{reg}}(\beta) = -\frac{i\hbar_{\text{eff}}}{T}\log\alpha_\beta. \tag{6}$$

- Once we have obtained the N_c values of $\varepsilon_{\text{eff}}^{\text{reg}}(\beta_m)$, we build explicitly the effective tight-binding Hamiltonian H_{eff}, whose coupling elements $t_n^{\text{eff}} \equiv \langle (m+n)_{\text{reg}}|H_{\text{eff}}|m_{\text{reg}}\rangle$ are computed from the discrete Fourier Transform:

$$t_n^{\text{eff}} = \frac{1}{N}\sum_{\beta_m} \varepsilon_{\text{eff}}^{\text{reg}}(\beta_m)\exp(i\beta_m\lambda n). \tag{7}$$

Dynamic evolution under the effective Hamiltonian

The effective Hamiltonian is a tight-binding model of N_c sites $|n\rangle$, with $n = 0, \dots N_c - 1$. The wavefunction $|\psi\rangle$ is propagated over two periods with effective evolution propagator:

$$|\psi(t+T)\rangle = U_{\text{eff}}\,|\psi(t)\rangle \quad \text{with} \quad U_{\text{eff}} = \exp\left(-i\frac{H_{\text{eff}}T}{\hbar_{\text{eff}}}\right), \tag{8}$$

obtained using a Padé approximation.

Construction of the regular Wannier-states

The Wannier states of the unperturbed lattice (with $\varepsilon = 0$) provide an approximation of the regular modes $|n_{\text{reg}}\rangle$ of the modulated lattice discussed in the letter. To construct them, we thus use a procedure similar to that used for the determination of the effective energy band, but using the unmodulated lattice (with $\varepsilon = 0$): For each value of $\beta_m = 2\pi m/(N_c\lambda)$, $m = 0, \dots N_c - 1$, we diagonalize the evolution operator over two periods $T = 4\pi$ and look for the eigenstate having the largest overlap with a Gaussian state centered on the regular island. The p representation of this eigenstate gives the coefficient of the Wannier state on the partial (uncomplete) grid $p = \hbar_{\text{eff}}\beta + n\delta p$ of size N_p. After repeating N_c times this procedure, we obtain the full p representation of the Wannier state (on the complete momentum basis of size N_pN_c).

Miscellaneous

The classical dynamics is simulated using a RK4 Runge-Kutta algorithm. Husimi phase-space representations are computed using the procedure described e.g. in [2].

Derivation of the hopping law for large system sizes

To derive the hopping law Eq. (3), we first decompose the effective Bloch band as a regular part ε_0 and a sum over all resonance terms:

$$\varepsilon_{\text{reg}}^{\text{eff}}(\beta) = \varepsilon_0(\beta) + \sum_{\text{resonances}} \varepsilon_{\asymp}(\beta - \beta_0, W, \alpha), \tag{9}$$

where each resonance is characterized by three parameters: β_0 the position of the resonance, W the coupling intensity between the chaotic and the regular state and α the slope of the energy of the involved chaotic state with β. Each

resonance can be described by a two-level Hamiltonian of an avoided crossing at $\beta = 0$:

$$\begin{pmatrix} \varepsilon_{\rm reg}(\beta) & W \\ W & \varepsilon_{\rm ch}(\beta) \end{pmatrix} \tag{10}$$

with $\varepsilon_{\rm reg}(\beta) = 0$ (since it is taken into account by ε_0 in Eq. (9)) and $\varepsilon_{\rm ch}(\beta) = \alpha\beta$. The corresponding eigenstates $|\beta_\pm\rangle$ and eigenenergies $\varepsilon_\pm(\beta)$ follow:

$$\varepsilon_\pm(\beta) = \frac{\varepsilon_{\rm reg} + \varepsilon_{\rm ch}}{2} \pm \sqrt{\Delta^2 + W^2} \quad \text{and} \quad |\beta_\pm\rangle = \begin{cases} \cos\theta\,|\beta_{\rm reg}\rangle + \sin\theta\,|\beta_{\rm ch}\rangle \\ -\sin\theta\,|\beta_{\rm reg}\rangle + \cos\theta\,|\beta_{\rm ch}\rangle \end{cases}, \tag{11}$$

with $\Delta = (\varepsilon_{\rm reg} - \varepsilon_{\rm ch})/2$ and $\theta \in [0, \pi/2]$ verifying $\tan 2\theta = |W|/\Delta$. The prescription for the effective spectrum construction is to select the energy associated with the eigenstate having the largest projection on the regular subspace. We thus get:

$$\varepsilon_\gtrless(\beta, W, \alpha) = \frac{\alpha}{2}\left(\beta - \mathrm{sgn}(\beta)\sqrt{\beta^2 + \left(\frac{2|W|}{\alpha}\right)^2}\right). \tag{12}$$

Taking the Fourier transform, we then have

$$t_n = t_n^0 + \sum_{\rm resonances} t_n^\gtrless(\beta_0, W, \alpha) \quad \text{with} \quad t_n^\gtrless(\beta_0, W, \alpha) = \frac{\lambda}{2\pi}\int_{-\pi/\lambda}^{\pi/\lambda} \varepsilon_\gtrless(\beta - \beta_0, W, \alpha)\mathrm{e}^{-in\beta\lambda}\,\mathrm{d}\beta\,. \tag{13}$$

We now assume that $\varepsilon_\gtrless(\beta - \beta_0, W, \alpha)$ is peaked around β_0 and that β_0 is sufficiently far from the edge of the boundary of the Brillouin zone, so that

$$t_n^\gtrless(\beta_0, W, \alpha) \approx \mathrm{e}^{in\beta_0\lambda}\frac{\lambda}{2\pi}\int_{-\pi/\lambda}^{\pi/\lambda} \varepsilon_\gtrless(\beta, W, \alpha)\mathrm{e}^{-in\beta\lambda}\,\mathrm{d}\beta\,. \tag{14}$$

The latter expression can be evaluated for large n values. We introduce $x = \beta\lambda$ and $\eta = 2\lambda|W|/\alpha = \lambda\Delta\beta/2$, it reads

$$t_n^\gtrless = \frac{\mathrm{e}^{in\beta_0\lambda}\alpha}{4\pi\lambda} \times \underbrace{\int_{-\pi}^{\pi}\left(x - \mathrm{sgn}(x)\sqrt{x^2+\eta^2}\right)\mathrm{e}^{-inx}\,\mathrm{d}x}_{I^*}, \tag{15}$$

we split the integral I (taking complex conjugation) in two parts, the first one gives

$$\int_{-\pi}^{\pi} x\mathrm{e}^{inx}\,\mathrm{d}x = \frac{2i\pi}{n}(-1)^{n+1}. \tag{16}$$

The second part can be rewritten

$$\int_0^{\pi} \mathrm{sgn}(x)\sqrt{x^2+\eta^2}\mathrm{e}^{inx}\,\mathrm{d}x - \text{c.c.}, \tag{17}$$

we then deform the contour of integration $0 \to \pi$ to a complex circuit $0 \to iT \to iT + \pi \to \pi$ with T some large real number. Using Watson's formula, the first part gives (setting $x = iy$)

$$i\int_0^T \sqrt{\eta^2 - y^2}\mathrm{e}^{-ny}\,\mathrm{d}y \sim \frac{i|\eta|}{n}. \tag{18}$$

The second part is negligible for T large enough (setting $x = y + iT$):

$$\mathrm{e}^{-nT}\int_0^{\pi} \sqrt{(y+iT)^2+\eta^2}\mathrm{e}^{-iny}\,\mathrm{d}y \to 0. \tag{19}$$

Using Watson's formula and assuming $\Delta\beta \ll \frac{2\pi}{\lambda}$ so that $(\eta/\lambda)^2 \ll 1$, the third part (setting $x = \pi + iy$) gives:

$$i(-1)^{n+1}\int_0^T \sqrt{(\pi+iy)^2+\eta^2}\mathrm{e}^{-ny}\,\mathrm{d}y \sim \frac{i\pi}{n}(-1)^{n+1}. \tag{20}$$

Putting all terms together (taking care of complex conjugation) we end up with

$$t_n^{\asymp} \approx \frac{\mathrm{e}^{in\beta_0\lambda}\alpha}{4\pi\lambda}\left(\frac{2i\pi}{n}(-1)^{n+1} - \frac{2i\eta}{n} - \frac{2i\pi}{n}(-1)^{n+1}\right)^* = \frac{\mathrm{e}^{in\beta_0\lambda}\alpha}{4\pi\lambda} \times \frac{i4\lambda|W|}{|\alpha|} = \frac{i}{\pi n}\mathrm{sgn}(\alpha)|W|\mathrm{e}^{in\beta_0\lambda}. \tag{21}$$

We finally assume that t_n^0 is negligible for large n values (because it decays exponentially), so that

$$t_n \approx \frac{i}{\pi n}\sum_{\text{resonances}} \mathrm{sgn}(\alpha)|W|\mathrm{e}^{in\beta_0\lambda}. \tag{22}$$

[1] M. Arnal, G. Chatelain, M. Martinez, N. Dupont, O. Giraud, D. Ullmo, B. Georgeot, G. Lemarié, J. Billy, and D. Guéry-Odelin, Science Advances **6**, eabc4886 (2020).

[2] M. Terraneo, B. Georgeot, and D. L. Shepelyansky, Phys. Rev. E **71**, 066215 (2005).